Published as: *Neuron*. 2012 September 6; 75(5): 799–809.

Atoh1 governs the migration of post-mitotic neurons that shape respiratory effectiveness at birth and chemoresponsiveness in adulthood

Wei-Hsiang Huang[1,4], **Srinivasan Tupal**[5], **Teng-Wei Huang**[1,4], **Christopher S. Ward**[2,4], **Jeffery L. Neul**[1,2,4], **Tiemo J. Klisch**[2,4], **Paul A. Gray**[5], and **Huda Y. Zoghbi**[1,2,3,4,*]

[1]Program in Developmental Biology, Baylor College of Medicine, Houston, Texas 77030, USA

[2]Department of Molecular and Human Genetics, Baylor College of Medicine, Houston, Texas 77030, USA

[3]Howard Hughes Medical Institute, Baylor College of Medicine, Houston, Texas 77030, USA

[4]Jan and Dan Duncan Neurological Research Institute at Texas Children's Hospital, Baylor College of Medicine, Houston, Texas 77030, USA

[5]Department of Anatomy and Neurobiology, Washington University School of Medicine, St. Louis, Missouri 63110, USA

SUMMARY

Hindbrain neuronal networks serving respiratory, proprioceptive, and arousal functions share a developmental requirement for the bHLH transcription factor *Atoh1*. Loss of *Atoh1* in mice results in respiratory failure and neonatal lethality; however, the neuronal identity and mechanism by which Atoh1-dependent cells sustain newborn breathing remains unknown. We uncovered that selective loss of *Atoh1* from the post-mitotic retrotrapezoid nucleus (RTN) neurons results in severely impaired inspiratory rhythm and pronounced neonatal death. Mice that escape neonatal death develop abnormal chemoresponsiveness as adults. Interestingly, the expression of *Atoh1* in the RTN neurons is not required for their specification or maintenance, but is important for their proper localization and to establish essential connections with the preBötzinger Complex (preBötC). These results provide insights into the genetic regulation of neonatal breathing and shed light on the labile sites that might contribute to sudden death in newborn infants and altered chemoresponsiveness in adults.

INTRODUCTION

Respiration is orchestrated by a multitude of hindbrain neurons that generate rhythm, modulate motor patterns, and monitor physiological states (Feldman and Del Negro, 2006; Feldman et al., 2003). In humans, aberrant respiratory control presents a significant public health burden, with sudden infant death syndrome being the leading cause of postnatal infant mortality. Moreover, genetic disorders such as Joubert syndrome and congenital central hypoventilation syndrome (CCHS) also impair central control of respiration, as does central

*Correspondence: hzoghbi@bcm.edu.

apnea in adults. However, our knowledge about the underlying transcriptional regulation of the neurocircuitries controlling respiration remains largely incomplete. In the case of CCHS, a polyalanine expansion in *paired-like homeobox 2b* (*PHOX2B*) − a transcription factor essential for the development of subsets of hindbrain motor neurons, interneurons, and post-ganglionic neurons of the sympathetic, parasympathetic and enteric nervous system − has been identified as the disease-defining mutation (Amiel et al., 2003). Mice carrying the most common *PHOX2B* mutation display neonatal lethality caused by central apnea (Dubreuil et al., 2008), which highlights the critical role of *Phox2b*-dependent hindbrain structures in newborn breathing.

While studying the functions of the bHLH transcription factor *atonal homolog 1* (*Atoh1*, also known as *Math1*) in hindbrain development, we discovered that *Atoh1*-null mice die within the first hour after birth from respiratory failure (Ben-Arie et al., 1997). *Atoh1* is expressed in the proliferating rhombic lip (RL) progenitors that give rise to hindbrain neuronal subtypes constituting the respiratory, interoceptive, proprioceptive, and arousal systems (Rose et al., 2009a). In addition, *Atoh1* is expressed in the post-mitotic RL-independent parafacial respiratory group / retrotrapezoid nucleus (hereafter referred to as the RTN) and paratrigeminal (pTRI) neurons that surround the facial motor nucleus (nVII) and trigeminal motor nucleus (nV), respectively (collectively termed paramotor neurons) (Dubreuil et al., 2009; Rose et al., 2009b; Smith et al., 1989; Stornetta et al., 2006). While *Atoh1* expression in the mitotic RL precursors is essential for their specification (Machold and Fishell, 2005; Wang et al., 2005), the physiological function of *Atoh1* in the post-mitotic RL-independent paramotor neurons is currently unknown. Many Atoh1-dependent neurons may provide modulatory inputs to the preBötzinger Complex (preBötC), the hypothesized primary inspiratory rhythm generator in mammals (Gray et al., 1999; Rose et al., 2009b; Smith et al., 1991). Because of *Atoh1*'s complex expression pattern, it is unclear which neuronal population is responsible for the respiratory and lethality phenotypes.

We used conditional inactivation, in combination with genetic neuronal projection mapping and electrophysiological studies, to explore the mechanism by which Atoh1 modulates respiration and to pinpoint the identity of the neurons critical for neonatal breathing. We uncovered the neuronal identity and mechanism by which Atoh1 mediates neonatal respiratory activity and revealed the function of Atoh1 during the development of RTN neurons that affect neonatal respiratory efficacy and respiratory chemoresponsiveness in adulthood.

RESULTS

The preBötC neurons receive Atoh1-dependent neuronal projections

Atoh1 null mice die shortly after birth, despite retaining the rhythmogenic preBötC populations and the capacity to generate respiratory output *in vitro* (Rose et al., 2009b). We set out to delineate Atoh1-dependent projections that innervate the preBötC by comparing wild type (WT) and *Atoh1* null mice, with a focus on Atoh1 populations adjacent to the preBötC (Figure 1A). To this end, we crossed mice that constitutively express Cre recombinase from the endogenous *Atoh1* locus ($Atoh1^{Cre/+}$) with $Atoh1^{+/-}$ mice that also carry a Cre-responsive $Tau^{mGFP\text{-}nLacZ}$ reporter allele. Upon Cre expression, nuclear LacZ (nLacZ) and myristoylated GFP (mGFP) permanently mark neuronal somas and projections, respectively in WT ($Atoh1^{Cre/+}$; $Tau^{mGFP\text{-}nLacZ}$) and *Atoh1*-null ($Atoh1^{Cre/-}$; $Tau^{mGFP\text{-}nLacZ}$) mice. Consistent with the observation that *Atoh1* is essential for the formation of RL descendants (Machold and Fishell, 2005; Wang et al., 2005), RL-derived Atoh1 populations in the ventral medulla, including the lateral reticular nucleus (LRt) and spinal trigeminal neurons (Sp5I), were virtually abolished in the *Atoh1*-null brainstem at E18.5 (Figure 1, compare C to B). In contrast, *Atoh1*-null mice still retain the RL-

independent RTN neurons, but the somas cluster at the dorsal surface of nVII, likely as a result of a migration defect (white arrowheads) (Figures 1B, C). Moreover, the closely localized nVII neurons, which do not express *Atoh1*, show normal marker expression and localization (Figures S1A, B), suggesting their development is Atoh1-independent.

During embryonic development, the RTN neurons migrate radially to assume their final location around the nVII, with the majority of them lining the ventral medullar surface (Dubreuil et al., 2009; Rose et al., 2009b). In *Atoh1*-null mice, the mislocalized RTN neurons retain expression of lineage markers such as *Phox2b* and *ladybird homeobox homolog 1* (*Lbx1*), similar to WT mice (Figures 1D, E), indicating that their lineage identities are unchanged. This defect is different from the CCHS mouse model, in which these neurons do not form (Dubreuil et al., 2008).

We then stained for myristoylated GFP to ask whether loss of *Atoh1* affects neuronal connectivity of lower brainstem circuitry. In the preBötC region (orange dotted circled neurons marked by somatostatin, Sst) of the E18.5 WT brainstem (Figure 1F), we detected neuronal processes extending from both rostral (white open arrowheads) and caudal (white arrowheads) Atoh1 populations. The rostral neuronal bundles correspond to the pontine Atoh1 respiratory populations and the RTN neurons, while the caudal processes belong predominantly to the LRt neurons (Abbott et al., 2009; Rose et al., 2009a; Rose et al., 2009b). This early connectivity is consistent with connectivity in adult rodents and functional connectivity occurring prior to the onset of inspiratory behaviors *in utero* (Feldman and Del Negro, 2006). In the *Atoh1*-null brain, the preBötC received little to no Atoh1-dependent rostral and caudal inputs (Figure 1G). Notably, neurites of the mislocalized RTN neurons accumulate at the dorsal side of nVII and do not extend to the preBötC. This suggests that *Atoh1*-null RTN neurons not only mislocalize but also lack direct targeting to the primary breathing center.

Atoh1 neurons within the *HoxA4* domain do not determine neonatal survival

In an effort to identify the Atoh1 subpopulations critical for neonatal survival, we applied conditional knockout strategies. We have previously shown that removal of *Atoh1* using a $HoxB1^{Cre}$ allele that covers all tissues caudal to the rhombomere 3/4 boundary results in 50% neonatal lethality (Maricich et al., 2009). Hence we focused on hindbrain Atoh1 lineages that fall within this region. The ventral medulla contains a number of Atoh1-dependent populations that may provide input to the respiratory column, including the trigeminal sensory inputs (Potts et al., 2005), the sub-caudal ventrolateral medulla neurons (Gray et al., 2010; Wang et al., 2002; Wang et al., 2003), and the LRt nucleus (Ezure and Tanaka, 1997). To evaluate whether loss of these caudal Atoh1 hindbrain populations contributes to the neonatal lethality of *Atoh1*-null mice, we generated a transgenic mouse model expressing Cre recombinase under the regulation of the *HoxA4* enhancer sequence (Behringer et al., 1993). Crossing $HoxA4^{Cre}$ to $Rosa^{LacZ/LacZ}$ reporter mice, we confirmed that the $HoxA4^{Cre}$ allele predominantly targets neurons caudal to the rhombomere 6/7 boundary, sparing anterior structures such as the RTN (Figures 2A-G). Mice carrying $HoxA4^{Cre}$ and *Atoh1-LacZ* (an *Atoh1*-null allele that traces Atoh1-expressing cells with LacZ, $HoxA4^{Cre}$; $Atoh1^{LacZ/+}$) were crossed with $Atoh1^{flox/flox}$ mice to delete *Atoh1* caudal to the rhombomere 6/7 boundary ($Atoh1^{HoxA4CKO}$: $HoxA4^{Cre}$; $Atoh1^{flox/LacZ}$). Fate mapping using X-gal staining confirmed that Atoh1 neurons of the posterior extramural stream, such as the LRt and external cuneate (ECu) nuclei, as well as radially migrating populations are ablated in $Atoh1^{HoxA4CKO}$ brainstems (Figures 2H, I). Because no conditional mutants showed lethality (0/25) at birth, and only three died at P1, we conclude that the caudally-derived Atoh1 lineages play a minor role in neonatal survival.

Atoh1 expression in the RTN is critical for neonatal survival and respiratory rhythmogenesis

The RTN neurons transiently express *Atoh1* (E12.0-P0) and are localized within the *HoxB1* domain (Dubreuil et al., 2009; Maricich et al., 2009; Rose et al., 2009b), making them candidate neurons account for the lethality observed in the $HoxB1^{Cre}$ conditional mutants. To determine whether *Atoh1* expression is cell-autonomously required for their proper migration and to evaluate the physiological role of post-mitotic *Atoh1* expression *in vivo*, we removed *Atoh1* from the *Phox2b*-derived paramotor neurons using $Phox2b^{Cre}$ transgenic mice (Rossi et al., 2011). Cre expression in $Phox2b^{Cre}$; $Rosa^{EYFP/+}$ mice showed more than 98% colocalization (quantified from 3 embryos) among EYFP, Phox2b, and Lbx1 in the RTN neurons (yellow arrowheads), confirming correct expression of Cre (Figure 3A).

Interestingly, the two groups of paramotor neurons displayed different requirements for Atoh1. $Phox2b^{Cre}$-mediated *Atoh1* conditional knockout ($Atoh1^{Phox2bKO}$) did not affect RTN lineage identity (retained Phox2b and Lbx1 expression, Figure 3B), but it did disrupt their normal radial migratory path towards the ventral brainstem (white arrowheads) (Figure 3B). Moreover, the expression of RTN differentiation marker, *neurokinin 1 receptor* (*NK1R*), is lost without *Atoh1* (Figure 3C), suggesting Atoh1 plays a cell-autonomous role in both RTN neuronal migration and differentiation. This phenotype is distinct from the induced expression of the alanine expanded *Phox2b* ($Phox2b^{27Ala}$) either systematically or in rhombomeres 3/5 where the RTN neurons are eliminated (Ramanantsoa et al., 2011). The paratrigeminal (pTRI) neurons surrounding the trigeminal motor nucleus (nV) also express *Atoh1, Phox2b* and *Lbx1* (Figure S2A). They are also targeted by the $Phox2b^{Cre}$ allele (Figure S2B) and showed Atoh1-independent lineage specification (Figure S2C). However, unlike the RTN neurons, the pTRI neurons do not require Atoh1 for proper localization, as shown by marker analyses (Figures S2D, E) and cell number quantification (Figure S2F) from serial sections. $Phox2b^{Cre}$-mediated conditional knockout do not affect RL-derived Atoh1 neurons, as mRNA *in situ* hybridization (Figure 4A) and fate mapping analyses (Figures 4B-E) showed that *Atoh1* expression and the development of RL populations are normal in the $Atoh1^{Phox2bCKO}$ mice. We conclude that $Atoh1^{Phox2bCKO}$ mice show a selective RTN mislocalization phenotype while the rest of the RL-derived Atoh1 populations remained unaffected.

We monitored the birth of conditional mutants and discovered that although the birth rate of all genotypes conformed to Mendelian ratios, 43% (20/46) of $Atoh1^{Phox2bCKO}$ mice died within the first hour after birth; none of the other genotypes showed postnatal lethality. We were surprised to find erroneous RTN migration in surviving $Atoh1^{Phox2bCKO}$ mice, similar to the mice that died at P0 (Figures S3A-D), suggesting that loss of *Atoh1* increases respiratory vulnerability specifically during the newborn period. To determine whether the RTN and caudal *HoxA4*-derived Atoh1 neurons affect newborn viability synergistically, we generated $Phox2b^{Cre}$; $HoxA4^{Cre}$-mediated *Atoh1* mutant animals, which showed neonatal lethality (52%, 9/17) not significantly different from that of $Phox2b^{Cre}$ alone (two-tailed p value=0.4477, Fisher's exact test). Taken together, we conclude that Atoh1-mediated development of the RTN neurons is critical for neonatal respiratory fitness.

To ascertain whether loss of *Atoh1* in the RTN has a direct effect on the respiratory rhythm-generating networks right before birth, we recorded the inspiratory activity from the C4 root of E18.5 brainstem-spinal cord preparations. Interestingly, the baseline fictive respiratory frequency of the $Atoh1^{Phox2bCKO}$ mice was significantly slower than that of their WT littermates ($Atoh1^{Phox2bCKO}$: 37.44 ± 2.48%, n=5, versus WT: 100 ± 22.24%, n=9, $p<0.05$) (Figure 5A). To test the response of respiratory circuit to excitatory neuropeptides, we recorded the inspiratory activity of WT and $Atoh1^{Phox2bCKO}$ brainstems 5 minutes before and after 1 μM Substance P (SP) treatment (Figure 5B). The $Atoh1^{Phox2bCKO}$ mice show

consistently depressed baseline motor activity when compared with WT (*Atoh1*^{Phox2bCKO}: 23.45 ± 5.60%, n=5, versus WT: 100 ± 34.61%, n=6, *p<0.05, paired t-test). Interestingly, SP application significantly increased the motor activity of WT (174.71 ± 39.32%, compared with WT before SP, n=6, *p<l0.05) but not *Atoh1*^{Phox2bCKO} preparations (16.55 ± 5.60%, compared with WT before SP, n=5, *p<0.05). These data suggest that Atoh1 is important for the RTN neurons to modulate inspiratory frequency, and the RTN neurons are a critical component of the neonatal rhythmogenic network.

Atoh1^{Phox2bCKO} mice develop abnormal respiratory chemoresponsiveness

The lifelong attenuated ventilatory response to hypercapnia is a major contributing factor to fatal apnea in CCHS patients. Such a chemosensory defect might be caused by functional impairments in *Phox2b*-dependent structures such as the carotid body and RTN neurons (Amiel et al., 2003; Dubreuil et al., 2008). Carotid bodies are the peripheral chemoreceptors that sense the arterial partial pressure of oxygen (pO_2) and, to a lesser extent, carbon dioxide (pCO_2), along with changes in pH. Although the cellular identities of central CO_2 chemoreceptors remain elusive, it has been shown that the RTN neurons are activated by low pH and can increase ventilation upon sensing high pCO_2 (Abbott et al., 2009; Mulkey et al., 2004).

The *en bloc* brainstem preparation responds to lower pH at early embryonic stages, allowing us to test the integrity of embryonic chemosensory network when the RTN is the only affected population. We first recorded inspiratory activities using E16.5 WT and *Atoh1*^{Phox2bCKO} embryos under baseline pH (7.4), and then perfused the brainstems using artificial cerebrospinal fluid (aCSF) with a lower pH (7.2). The *Atoh1*^{Phox2bCKO} embryos show a slower baseline behavior when compared with WT (*Atoh1*^{Phox2bCKO}: 58.43 ± 2.24%, n=11, versus WT: 100 ± 7.14%, n=7, p<0.001), consistent with a role for RTN in modulating embryonic inspiratory rhythmogenicity. Interestingly, both WT and *Atoh1*^{Phox2bCKO} preparations are sensitive to lower pH (*Atoh1*^{Phox2bCKO}: 227.32 ± 4.99% versus WT: 251.00 ± 5.31%, both compared to baseline WT, p<0.001) (Figure 5C). These results indicate that the chemosensory circuits of the *Atoh1*^{Phox2bCKO} embryos are still capable to detect pH change at early embryonic stage and is distinct from the effects of RTN deletion in the *Egr-2* lineages by expressing *Phox2b*^{27Ala} (Ramanantsoa et al., 2011).

Normally, the RTN neurons are located at the marginal layer of ventral brainstem where blood vessels deliver CO_2 signals (Lazarenko et al., 2009). To determine whether RTN mislocalization affects CO_2 detection in free-moving adult animals, we utilized unrestrained whole body plethysmography to monitor the respiration of 3-month-old *Atoh1*^{Phox2bCKO} survivor mice. The breathing parameters of *Atoh1*^{Phox2bCKO} mice (n=9) and their littermates (WT, n=21) were indistinguishable at rest, but when challenged with hypercapnia (5% CO_2), WT mice showed increased respiratory frequency (RF, 340.92 ± 3.79 min^{-1}), tidal volume (V_T, 13.73 ± 0.30 $\mu l \cdot g^{-1}$), and minute ventilation (V_E, 4.68 ± 0.13 $ml \cdot min^{-1} \cdot g^{-1}$) (Figure 6A). In contrast, the *Atoh1*^{Phox2bCKO} mice showed a significantly attenuated response to hypercapnia, as reflected by modest increases in RF (286.45 ± 9.86 min^{-1}), V_T (10.10 ± 0.45 $\mu l \cdot g^{-1}$), and V_E (2.97 ± 0.19 $ml \cdot min^{-1} \cdot g^{-1}$) (Figure 6A). The compromised hypercapnic response might be due to the inability of the RTN neurons to detect changes in pCO_2 and trigger respiration owing to their failed migration. At the same time, the partially preserved hypercapnic response implies that the carotid bodies are spared. To test if the carotid bodies are functionally intact, we challenged *Atoh1*^{Phox2bCKO} mice (n=9) and their littermates (WT, n=21) with hypoxic gas (10% O_2). Interestingly, *Atoh1*^{Phox2bCKO} mice displayed a stronger hypoxia-evoked ventilatory response than WT (RF: 346.63 ± 14.36 versus 286.53 ± 4.75 min^{-1}; V_T: 12.8 ± 0.74 versus 11.05 ± 0.34 $\mu l \cdot g^{-1}$; V_E: 4.5 ± 0.33 versus 3.11 ± 0.11 $ml \cdot min^{-1} \cdot g^{-1}$) (Figure 6B), suggesting that the O_2-sensing carotid bodies could provide compensatory feedback. Overall, our results demonstrate that transient *Atoh1*

expression in post-mitotic RTN neurons is critical for mediating respiratory chemoresponsiveness in free-moving adult mice, most likely through promoting their ventral localization.

DISCUSSION

This study has yielded three important findings. First, *Atoh1* expression in the RTN neurons is critical for neonatal survival. Second, expression of *Atoh1* in the post-mitotic RTN neurons directs their migration through the embryonic hindbrain and establishes the connectivity that provides excitatory drive crucial for commencing inspiratory rhythm at birth. This cell-autonomous role for Atoh1 in RTN migration provides a mechanism by which derailed hindbrain development can result in disordered neonatal breathing and highlights the importance of the RTN neurons at this stage. Third, Atoh1-mediated RTN development at an early embryonic stage is necessary for normal respiratory chemosensitivity in the adult.

Genetic removal of *Atoh1* from the *Phox2b* neurons results in nearly 50% neonatal lethality and indicates that even transient *Atoh1* embryonic expression plays a major role in neonatal respiration. Given that the glutamatergic RTN neurons have been hypothesized to entrain the embryonic preBötC (Bochorishvili et al., 2012; Thoby-Brisson et al., 2009), we proposed that the migration defect in the $Atoh1^{Phox2bCKO}$ mice and the consequent loss of synaptic contact dramatically decreases excitatory input, thereby challenging the neonatal respiratory rhythm-generating network (Feldman et al., 2003; Mellen et al., 2003). Support for this contention comes from the ability of $Atoh1^{Phox2bCKO}$ *en bloc* preparations to still generate respiratory rhythm (albeit depressed), which confirms the participation of RTN neurons in neonatal respiratory rhythm modulation. Once the conditional mutants survive past P0, they do not show additional lethality, similar to the partially penetrant neonatal lethality of the *Egr-2* null mice (~ 50% at P0) (Jacquin et al., 1996). The preBötC thus appears to become a more independent rhythmogenic center postnatally. The extensive reorganization in rhombomeres 3 and 5 of the *Egr-2* null mice eliminates most RTN neurons (Thoby-Brisson et al., 2009), but neurons outside of *Egr-2* domain may compensate for the lethality caused by loss of RTN neurons. In our case, we propose that some of the RL-derived Atoh1 neurons could function collectively as a second excitatory source for the preBötC, which might stochastically reach the excitatory threshold to allow survival of half the newborn $Atoh1^{Phox2bCKO}$ mice.

Although the paratrigeminal neurons are anatomically intact without *Atoh1*, their role in respiratory control remains unknown, and we do not exclude the possibility that they modulate breathing in an Atoh1-dependent manner. RL-independent and dependent Atoh1-positive neuronal subpopulations might each contribute to neonatal respiratory activity to a similar extent. Fifty percent of newborn mice with *Atoh1* deletion in the *Wnt*-1 lineages, which affect most of the RL-derived neurons, die within 24–36 hours of birth (Morrison et al., 2009), which lends further support to this hypothesis.

Loss of *Atoh1* causes aberrant RTN neuronal migration, analogous to the consequence of loss of *atonal* during the development of the *Drosophila* dorsal cluster (DC) neurons. *Atonal* is expressed in the post-mitotic DC neurons that innervate the optic lobes (Hassan et al., 2000); in its absence, the DC neurons are still present, but are aberrantly positioned and show severely impaired target innervation and loss of axonal arborization. *Atonal* thus does not act as a classical proneural gene in the DC neurons. Interestingly, the ability of atonal/Atoh1 to control cell positioning and target innervation is limited to the few populations where these bHLH factors are expressed post-mitotically.

The identity of central chemoreceptors and the mechanism by which they detect elevated pCO_2 and stimulate breathing remain unclear, but these questions are currently under intense investigation (Guyenet, 2012). The *Atoh1*^{Phox2bCKO} surviving mice provide an unexpected opportunity to assess the extent to which mislocalized RTN neurons affect adult chemoresponsiveness. We observed that the *Atoh1*^{Phox2bCKO} surviving mice develop a significantly impaired hypercapnic response and hypersensitivity to hypoxia, suggesting that despite the possible development of compensatory mechanisms, the Atoh1-mediated development of the RTN neurons remains a crucial step that assures proper chemosensory response throughout life. During embryonic stage, the fictive motor activity of *Atoh1*^{Phox2bCKO} embryos is significantly slower than WT embryos under both baseline and pH challenge; but unlike the CCHS mouse models that lose the RTN and express *Phox2b*^{27Ala} in multiple brain regions (Dubreuil et al., 2008; Ramanantsoa et al., 2011), the pH response is virtually unchanged in the *Atoh1*^{Phox2bCKO} embryos. Thus the function of RTN neurons in rhythmogenic output can be separated from their chemosensory capacity, and it is unclear how the chemosensitive signal is transferred to respiratory network *in vitro*. Our *in vivo* experiment delivers CO_2 in a physiological context, and indicates that proper localization of the RTN to the highly vascularized ventral brainstem surface (where chemosensitive astrocytes reside) (Gourine et al., 2010) is critical for adult chemoresponsiveness. Whether the blunted chemosensitivity in the adult mouse is due to cell-autonomous deficits in RTN neurons and/or their displacement away from the ventral surface vascular bed and chemosensitive astrocytes is unknown. Furthermore, it is interesting to note that adult mice conditionally expressing the CCHS-causing *PHOX2B* mutation in the *Egr-2* domain also show a partially impaired hypercapnic response and hypersensitivity to hypoxia due to increased synaptic input from the carotid bodies (Ramanantsoa et al., 2011). This crosstalk between central and peripheral chemosensory systems warrants further investigation, as disturbance in blood gas homeostasis and failure to arouse from sleep are serious detriments to health.

Several bHLH transcription factors have emerged as disease-defining genes or genetic modifiers for neonatal respiratory disorders. Mutations in the *transcription factor 4* (*TCF4*, an Atoh1-interacting bHLH factor) cause Pitt-Hopkins syndrome, which manifests with infantile-onset hyperventilation (Amiel et al., 2007). Heterozygous nucleotide substitutions in *human achaete-scute homolog-1* of CCHS patients have been uncovered and might impair noradrenergic neural development (de Pontual et al., 2003). Both *TCF4* and *achaete-scute homolog-1* null mice die during the newborn period because of unknown breathing and feeding defects (Guillemot et al., 1993; Zhuang et al., 1996). In light of these dramatic phenotypes, studying conditional mutants of these bHLH factors will facilitate the identification of additional neuronal structures that ensure proper respiratory activity in the early postnatal life.

In sum, we provide direct evidence that the expression of *Atoh1* in the post-mitotic RTN neurons during fetal hindbrain development serves as an intrinsic signal that guides proper neuronal migration and projection, which is a critical step to stimulate inspiratory rhythm at birth. Selective loss of paramotor *Atoh1* expression compromises neonatal breathing and adult hypercapnic response. These findings provide an example of how transient expression of a bHLH transcription factor shapes the physiological function of post-mitotic neurons and provide insights into the developmental assembly of respiratory network that might be altered in neonatal respiratory disorders. Moreover, these data suggest that early developmental abnormalities, if survived, have an impact on physiological responses and respiratory health in adults.

EXPERIMENTAL PROCEDURES

Mice

Animal housing, husbandry, and euthanasia were conducted under the guidelines of the Center for Comparative Medicine, Baylor College of Medicine. See Supplemental Experimental Procedures for details on mouse models used.

Generation of the *HoxA4^{Cre}* transgenic mice

Using the Gateway system, three PCR fragments were generated: *HoxA4* responsive element (including exon 1 and part of exon 2, primers: HoxA4-for

5'-GGGGACAAGTTTGTACAAAAAAGCAGGCT*GGTACC*AAGTGTATATTCAGTGGTA AA-3', HoxA4-rev

5'-GGGGACCACTTTGTACAAGAAAGCTGGGT*TGCGCA*TGAATTCCTTCTCCAGTTC CAAG-3'), *Cre* sequence (primers: Cre-for

5'-GGGGACAAGTTTGTACAAAAAAGCAGGCT*TGGCCA*AGAAGAAGAGGAAGGTGT CC-3', Cre-rev

5'-GGGGACCACTTTGTACAAGAAAGCTGGGT*ACTAGT*CTAATCGCCATCTTCCAGC AG-3'), and an intron and polyadenylation signal taken from the mouse *Protoamine1* sequence (primers: PolyA-for

5'-GGGGACAAGTTTGTACAAAAAAGCAGGCT*ACTAGT*CCAGATACCGATGCTGCCG -3', PolyA-rev

5'-GGGGACCACTTTGTACAAGAAAGCTGGGT*GGTACC*GTACAGGTGGCTTGGTAG TCAATATTG-3'). The individual Gateway sequences are underlined, restriction enzyme sites are in italics. The fragments were cloned into the pDONR223 vector (Invitrogen) to yield a transgene consisting of the *HoxA4* enhancer/promoter, *Cre* sequence fused in-frame with the *HoxA4* sequence at exon 2, and the polyadenylation signal. The transgene was excised with KpnI and used in a pronuclear injection to generate transgenic mice according to standard procedures. Two transgenic lines were mated to FVB wild type mice for three to four generations before Cre expression analysis, which was carried out for two successive generations to confirm stable transmission. Both lines were maintained and line 2 is used in this study.

Immunofluorescence (IF) assay

IF and cryosectioning were performed as previously described (Rose et al., 2009b). Frozen sections were cut at 25 μm for soma analysis or 50 μm for projection analysis. The primary antibodies used are: chicken anti-β-gal (1:1000, Abcam), chicken anti-GFP (1:1000, Abcam), rabbit anti-Sst (1:500, Immunostar), rabbit anti-NK1R (1:500, Advanced Targeting Systems), goat anti-Phox2b (1:500, Santa Cruz), guinea pig anti-Lbx1 (1:10000, gift from C. Birchmeier). Secondary antibodies were conjugated with Alexa Fluor 488 or 555 (1:2000, Molecular Probes). We used a Leica TCS SP5 confocal system to detect fluorescent staining. Image brightness and contrast were normalized using Image J and Adobe Photoshop.

X-gal staining and *in situ* hybridization

Embryos prepared for X-gal staining were harvested, rinsed, and fixed in 4% paraformaldehyde for 20 minutes on ice. Embryos were washed three times for 10 minutes and pre-incubated with X-gal buffer (0.02% NP-40, 0.01% Sodium Deoxycholate, 5 mM Potassium Ferricyanide, 5 mM Potassium Ferrocyanide, in 1X phosphate buffered saline (PBS)) for 15 minutes in the dark, and then incubated with X-gal buffer containing 1 mg/ml X-gal (Gold Biotechnology). After sufficient staining (usually within 18–24 hours) at 37°C in the dark, specimens were washed three times for 10 minutes with PBS, post-fixed overnight at 4°C, washed again and stored in 30% sucrose/PBS at 4°C prior to OCT-embedded sectioning (25 μm). Whole mount embryos were viewed with a Lumar V12 stereoscope, slides with an Axioplan2 microscope, and images captured using Axiovision software (all Zeiss, Germany). For *in situ* hybridization, embryos were collected, rinsed, and freshly embedded for serial cryosectioning (20 μm). Sections were air-dried for 30 minutes prior to storage (−20°C). Probes were amplified from reverse-transcribed cDNA collected from embryonic C57/B6 brainstem by using primers from the Allen Brain Atlas (www.brain-map.org).

Neonatal *en bloc* preparations (E18.5)

Atoh1^{Phox2bCKO} (*Phox2b*^{Cre}; *Atoh1*$^{flox/LacZ}$) mice and their littermates (WT) were delivered by cesarean section on embryonic day 18.5 from anesthetized (ketamine/xylazine mixture) timed-pregnant animals. Standard brainstem-spinal (*en bloc*) preparations with an anterior transection near diencephalon-midbrain junction were made from them, which rostrally included cerebellum, pons and medulla, and extended caudally up to the sacral region of the spinal cord, while submerged in cold (4°C) artificial cerebral spinal fluid (aCSF: 124 mM NaCl, 3 mM KCl, 1.5 mM $CaCl_2$, 1 mM $MgSO_4$, 25 mM $NaHCO_3$, 0.5 mM NaH_2PO_4, 30 mM D-Glucose (all Sigma, St. Louis, USA) equilibrated with 95% O_2 and 5% CO_2 to pH=7.4). The preparations were transferred into a partitioned recording chamber with a rostral (~2 ml) and a caudal (~4 ml) spinal cord compartment that were gravity fed by separate reservoirs of heated (25–26°C) and aerated (95% O_2 and 5% CO_2) aCSF at a rate of 3–4 ml/min. These compartments were rendered mutually impervious by plugging the passage connecting the two compartments with paraffin wax. The preparations were allowed to stabilize in the chamber for ~30 minutes in circulating (rate 3–4 ml/minutes) aerated aCSF (25–26°C). Extracellular electrophysiological recording were made from C2-C6 ventral spinal motor roots using a suction electrode. The recordings were amplified using a low-noise differential amplifier (Grass Instruments) with band pass filtering (0.3–3 kHz). The signals were acquired at a rate of 4 kHz and digitized using an analog to digital converter (AD instruments, Colorado Springs, CO). Signal processing that included digital filtration (high-pass, cut-off frequency=0.3 Hz) and integration over time (absolute value with a 100 ms decay time constant) was done using LabChart 7 Pro software (Version 7.2.4, AD Instruments). After recording baseline activity, 1 μM Substance P (SP) was added to the rostral brainstem compartment. Peak times of the integrated bursts were determined and respiratory frequencies (bursts/min) were calculated. For statistical comparisons the fictive respiratory frequencies during baseline and SP application of all animals were expressed as percent normalized frequency using the mean baseline cervical burst frequency of WT (cervical burst frequency / mean baseline cervical burst frequency in wild type mice × 100). The percent normalized frequencies from WT and *Atoh1*^{Phox2bCKO} mice during baseline and application of SP were compared using independent samples t- and paired t-test, respectively. Paired t-test was used while comparing the baseline and effect of SP from 5 minutes traces within each genotype, whereas independent samples t-test was used for comparing between the groups. Statistical significance was accepted at a p-value lower than 0.05 for all comparisons.

Embryonic *en bloc* preparations (E16.5)

In vitro brainstem and cervical spinal cord preparations were generated from cesarean section isolated E16.5 embryos. Embryos were maintained in oxygenated artificial cerebrospinal fluid (aCSF) at 10–15 °C until dissection. Dissections were done under cold (4°C) aCSF (120 mM NaCl, 8 mM KCl, 1.26 mM $CaCl_2$, 1.5 mM $MgCl_2$, 21 mM $NaHCO_3$, 0.58 mM NaH_2PO_4, 30 D-Glucose, all Sigma, St. Louis, USA) equilibrated with 95% O_2 and 5% CO_2 to pH 7.4. Preparations were transferred into a 6 ml recording chamber and superfused by gravity perfusion method at a flow rate of 4 ml/min using aCSF solution at 30°C. Extracellular electrophysiological recording of fictive inspiratory bursts was made from the C1-C4 ventral spinal motor roots using glass suction electrodes. Signals were amplified, filtered, and recorded using a digital converter (AD instruments, Colorado Springs, CO). After recording the baseline activity for over 30 min, the effect of pH on the frequency of cervical bursts was studied by switching to aCSF (pH 7.2, 10.5 mM $NaHCO_3$, 130.5 mM NaCl) for over 30 min. Cervical fictive respiratory burst frequencies during baseline and application of lower pH aCSF in all the animals were expressed as normalized periods using the mean baseline cervical burst period of wild type mice (WT), and statistical comparisons were made using independent-samples t-test. The normalized periods were transformed to frequency. Statistical significance was accepted at a p-value lower than 0.001.

Unrestrained Whole Body Plethysmography (UWBP)

Three-month old male mice were placed within the UWBP chamber (Buxco), with a continuous flow rate of 1 L/min flushing the chambers with fresh air. Breath waveforms and derived parameters, including the instantaneous breathing rate, tidal volume, inspiratory time, and expiratory time, were identified and calculated with Biosystem XA software (Buxco). Mice were allowed to acclimate for 30 minutes, and breathing was recorded for 20 minutes (baseline). No significant differences were found between any respiratory parameter of the $Atoh1^{flox/LacZ}$, $Atoh1^{flox/+}$, and $Phox2b^{Cre}$; $Atoh1^{flox/+}$ mice, hence they were grouped as WT. To determine response to hypercapnic gas, the chamber was flushed with hypercapnic gas (5% CO_2) for 4 minutes after which breathing was recorded for 5 minutes of hypercapnic exposure (exposure), and allowed to recover in fresh air for 15 minutes (recovery). Hypoxic gas (10% O_2) challenge was done in the same manner. Breathing parameters for $Atoh1^{Phox2bCKO}$ ($Phox2b^{Cre}$; $Atoh1^{flox/LacZ}$) mice (n=9) and WT (n=21) were determined as the average instantaneous value over the recorded interval and averaged across 3 independent trials. To reduce artifacts from excessive movement and sniffing behavior, breaths that exhibited an inspiratory time less than 0.03 seconds, an expiratory time greater than 10 seconds, and a calculated exhaled tidal volume over 150% or under 50% of calculated inhaled tidal volume were excluded; recording were then split into 1 minute intervals and only those minutes during which the animal spent less than 10% of its breaths above 500 breaths per minute were included in the analysis. Parametric statistics were performed using ANOVA with genotype as a factor and significance was accepted at a p-value lower than 0.05.

Supplementary Material

Refer to Web version on PubMed Central for supplementary material.

Acknowledgments

We thank Drs. J. Elmquist, L. Gan, and C. Birchmeier for the $Phox2b^{Cre}$ and $Atoh1^{Cre}$ mice, and Lbx1 antibody, respectively. We also thank V. Brandt for editorial input. This work was supported by American Heart Association SouthWest affiliate Predoctoral Fellowship to W.H.H. (11PRE6080004); National Research Service Award to C.S.W. (NS066601); the Gene Expression and Microscopy Cores of the Baylor College of Medicine-Intellectual

and Developmental Disabilities Research Center (HD24064); Cancer Prevention Research Institute of Texas to T.J.K. (RP110390); National Heart, Lung, and Blood Institute to S.T. and P.A.G. (R01HL089742); and Howard Hughes Medical Institute to H.Y.Z.

REFERENCES

Abbott SB, Stornetta RL, Fortuna MG, Depuy SD, West GH, Harris TE, Guyenet PG. Photostimulation of retrotrapezoid nucleus phox2b-expressing neurons in vivo produces long-lasting activation of breathing in rats. J Neurosci. 2009; 29:5806–5819. [PubMed: 19420248]

Amiel J, Laudier B, Attie-Bitach T, Trang H, de Pontual L, Gener B, Trochet D, Etchevers H, Ray P, Simonneau M, et al. Polyalanine expansion and frameshift mutations of the paired-like homeobox gene PHOX2B in congenital central hypoventilation syndrome. Nat Genet. 2003; 33:459–461. [PubMed: 12640453]

Amiel J, Rio M, de Pontual L, Redon R, Malan V, Boddaert N, Plouin P, Carter NP, Lyonnet S, Munnich A, Colleaux L. Mutations in TCF4, encoding a class I basic helix-loop-helix transcription factor, are responsible for Pitt-Hopkins syndrome, a severe epileptic encephalopathy associated with autonomic dysfunction. Am J Hum Genet. 2007; 80:988–993. [PubMed: 17436254]

Behringer RR, Crotty DA, Tennyson VM, Brinster RL, Palmiter RD, Wolgemuth DJ. Sequences 5' of the homeobox of the Hox-1.4 gene direct tissue-specific expression of lacZ during mouse development. Development. 1993; 117:823–833. [PubMed: 8100763]

Ben-Arie N, Bellen HJ, Armstrong DL, McCall AE, Gordadze PR, Guo Q, Matzuk MM, Zoghbi HY. Math1 is essential for genesis of cerebellar granule neurons. Nature. 1997; 390:169–172. [PubMed: 9367153]

Bochorishvili G, Stornetta RL, Coates MB, Guyenet PG. Pre-Botzinger complex receives glutamatergic innervation from galaninergic and other retrotrapezoid nucleus neurons. J Comp Neurol. 2012; 520:1047–1061. [PubMed: 21935944]

de Pontual L, Nepote V, Attie-Bitach T, Al Halabiah H, Trang H, Elghouzzi V, Levacher B, Benihoud K, Auge J, Faure C, et al. Noradrenergic neuronal development is impaired by mutation of the proneural HASH-1 gene in congenital central hypoventilation syndrome (Ondine's curse). Hum Mol Genet. 2003; 12:3173–3180. [PubMed: 14532329]

Dubreuil V, Ramanantsoa N, Trochet D, Vaubourg V, Amiel J, Gallego J, Brunet JF, Goridis C. A human mutation in Phox2b causes lack of CO2 chemosensitivity, fatal central apnea, and specific loss of parafacial neurons. Proc Natl Acad Sci U S A. 2008; 105:1067–1072. [PubMed: 18198276]

Dubreuil V, Thoby-Brisson M, Rallu M, Persson K, Pattyn A, Birchmeier C, Brunet JF, Fortin G, Goridis C. Defective respiratory rhythmogenesis and loss of central chemosensitivity in Phox2b mutants targeting retrotrapezoid nucleus neurons. J Neurosci. 2009; 29:14836–14846. [PubMed: 19940179]

Ezure K, Tanaka I. Convergence of central respiratory and locomotor rhythms onto single neurons of the lateral reticular nucleus. Exp Brain Res. 1997; 113:230–242. [PubMed: 9063709]

Feldman JL, Del Negro CA. Looking for inspiration: new perspectives on respiratory rhythm. Nat Rev Neurosci. 2006; 7:232–242. [PubMed: 16495944]

Feldman JL, Mitchell GS, Nattie EE. Breathing: rhythmicity, plasticity, chemosensitivity. Annu Rev Neurosci. 2003; 26:239–266. [PubMed: 12598679]

Gourine AV, Kasymov V, Marina N, Tang F, Figueiredo MF, Lane S, Teschemacher AG, Spyer KM, Deisseroth K, Kasparov S. Astrocytes control breathing through pH-dependent release of ATP. Science. 2010; 329:571–575. [PubMed: 20647426]

Gray PA, Hayes JA, Ling GY, Llona I, Tupal S, Picardo MC, Ross SE, Hirata T, Corbin JG, Eugenin J, Del Negro CA. Developmental origin of preBotzinger complex respiratory neurons. J Neurosci. 2010; 30:14883–14895. [PubMed: 21048147]

Gray PA, Rekling JC, Bocchiaro CM, Feldman JL. Modulation of respiratory frequency by peptidergic input to rhythmogenic neurons in the preBotzinger complex. Science. 1999; 286:1566–1568. [PubMed: 10567264]

Guillemot F, Lo LC, Johnson JE, Auerbach A, Anderson DJ, Joyner AL. Mammalian achaete-scute homolog 1 is required for the early development of olfactory and autonomic neurons. Cell. 1993; 75:463–476. [PubMed: 8221886]

Guyenet P. How does CO2 activate the neurons of the retrotrapezoid nucleus. J Physiol. 2012; 590:2183–2184. [PubMed: 22589206]

Hassan BA, Bermingham NA, He Y, Sun Y, Jan YN, Zoghbi HY, Bellen HJ. atonal regulates neurite arborization but does not act as a proneural gene in the Drosophila brain. Neuron. 2000; 25:549–561. [PubMed: 10774724]

Jacquin TD, Borday V, Schneider-Maunoury S, Topilko P, Ghilini G, Kato F, Charnay P, Champagnat J. Reorganization of pontine rhythmogenic neuronal networks in Krox-20 knockout mice. Neuron. 1996; 17:747–758. [PubMed: 8893031]

Lazarenko RM, Milner TA, Depuy SD, Stornetta RL, West GH, Kievits JA, Bayliss DA, Guyenet PG. Acid sensitivity and ultrastructure of the retrotrapezoid nucleus in Phox2b-EGFP transgenic mice. J Comp Neurol. 2009; 517:69–86. [PubMed: 19711410]

Machold R, Fishell G. Math1 is expressed in temporally discrete pools of cerebellar rhombic-lip neural progenitors. Neuron. 2005; 48:17–24. [PubMed: 16202705]

Maricich SM, Xia A, Mathes EL, Wang VY, Oghalai JS, Fritzsch B, Zoghbi HY. Atoh1-lineal neurons are required for hearing and for the survival of neurons in the spiral ganglion and brainstem accessory auditory nuclei. J Neurosci. 2009; 29:11123–11133. [PubMed: 19741118]

Mellen NM, Janczewski WA, Bocchiaro CM, Feldman JL. Opioid-induced quantal slowing reveals dual networks for respiratory rhythm generation. Neuron. 2003; 37:821–826. [PubMed: 12628172]

Morrison KM, Miesegaes GR, Lumpkin EA, Maricich SM. Mammalian Merkel cells are descended from the epidermal lineage. Dev Biol. 2009; 336:76–83. [PubMed: 19782676]

Mulkey DK, Stornetta RL, Weston MC, Simmons JR, Parker A, Bayliss DA, Guyenet PG. Respiratory control by ventral surface chemoreceptor neurons in rats. Nat Neurosci. 2004; 7:1360–1369. [PubMed: 15558061]

Potts JT, Rybak IA, Paton JF. Respiratory rhythm entrainment by somatic afferent stimulation. J Neurosci. 2005; 25:1965–1978. [PubMed: 15728836]

Ramanantsoa N, Hirsch MR, Thoby-Brisson M, Dubreuil V, Bouvier J, Ruffault PL, Matrot B, Fortin G, Brunet JF, Gallego J, Goridis C. Breathing without CO(2) chemosensitivity in conditional Phox2b mutants. J Neurosci. 2011; 31:12880–12888. [PubMed: 21900566]

Rose MF, Ahmad KA, Thaller C, Zoghbi HY. Excitatory neurons of the proprioceptive, interoceptive, and arousal hindbrain networks share a developmental requirement for Math1. Proc Natl Acad Sci U S A. 2009a; 106:22462–22467. [PubMed: 20080794]

Rose MF, Ren J, Ahmad KA, Chao HT, Klisch TJ, Flora A, Greer JJ, Zoghbi HY. Math1 is essential for the development of hindbrain neurons critical for perinatal breathing. Neuron. 2009b; 64:341–354. [PubMed: 19914183]

Rossi J, Balthasar N, Olson D, Scott M, Berglund E, Lee CE, Choi MJ, Lauzon D, Lowell BB, Elmquist JK. Melanocortin-4 receptors expressed by cholinergic neurons regulate energy balance and glucose homeostasis. Cell Metab. 2011; 13:195–204. [PubMed: 21284986]

Smith JC, Ellenberger HH, Ballanyi K, Richter DW, Feldman JL. Pre-Botzinger complex: a brainstem region that may generate respiratory rhythm in mammals. Science. 1991; 254:726–729. [PubMed: 1683005]

Smith JC, Morrison DE, Ellenberger HH, Otto MR, Feldman JL. Brainstem projections to the major respiratory neuron populations in the medulla of the cat. J Comp Neurol. 1989; 281:69–96. [PubMed: 2466879]

Stornetta RL, Moreira TS, Takakura AC, Kang BJ, Chang DA, West GH, Brunet JF, Mulkey DK, Bayliss DA, Guyenet PG. Expression of Phox2b by brainstem neurons involved in chemosensory integration in the adult rat. J Neurosci. 2006; 26:10305–10314. [PubMed: 17021186]

Thoby-Brisson M, Karlen M, Wu N, Charnay P, Champagnat J, Fortin G. Genetic identification of an embryonic parafacial oscillator coupling to the preBotzinger complex. Nat Neurosci. 2009; 12:1028–1035. [PubMed: 19578380]

Wang H, Germanson TP, Guyenet PG. Depressor and tachypneic responses to chemical stimulation of the ventral respiratory group are reduced by ablation of neurokinin-1 receptor-expressing neurons. J Neurosci. 2002; 22:3755–3764. [PubMed: 11978851]

Wang H, Weston MC, McQuiston TJ, Stornetta RL, Guyenet PG. Neurokinin-1 receptor-expressing cells regulate depressor region of rat ventrolateral medulla. Am J Physiol Heart Circ Physiol. 2003; 285:H2757–H2769. [PubMed: 12933345]

Wang VY, Rose MF, Zoghbi HY. Math1 expression redefines the rhombic lip derivatives and reveals novel lineages within the brainstem and cerebellum. Neuron. 2005; 48:31–43. [PubMed: 16202707]

Zhuang Y, Cheng P, Weintraub H. B-lymphocyte development is regulated by the combined dosage of three basic helix-loop-helix genes, E2A, E2-2, and HEB. Mol Cell Biol. 1996; 16:2898–2905. [PubMed: 8649400]

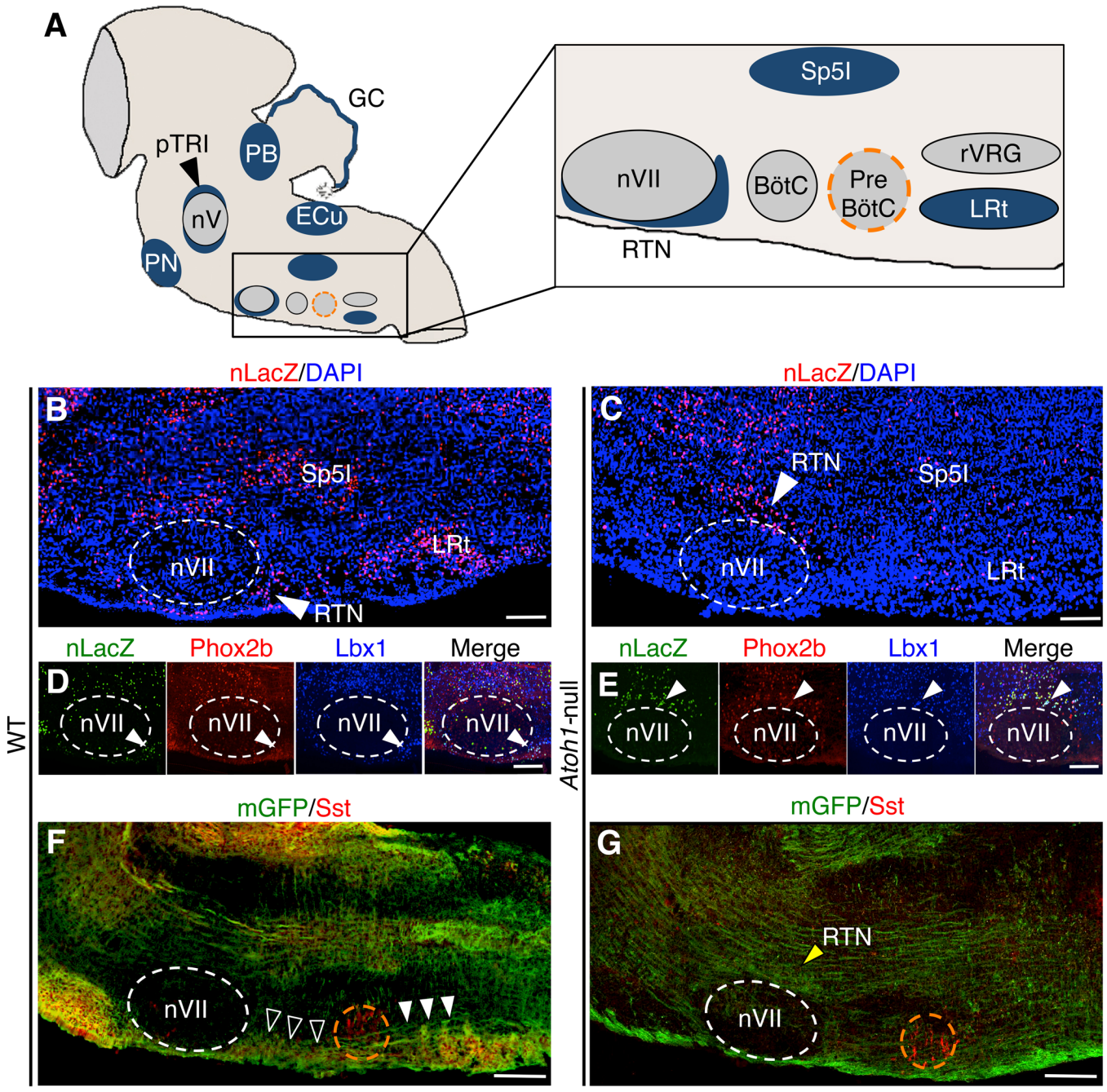

Figure 1. Brainstem neurons connect to the preBötC in an Atoh1–dependent manner

(A) Schematic representationofAtoh1–expressingneurons (in blue) in a sagittal plane of the E18.5 hindbrain. Rostral is left; PB: parabrachial, pTRI: paratrigeminal, GC: granule cells, PN: pontine, nV: trigeminal motor, ECu: external cuneate, Sp5I: spinal trigeminal, RTN: retrotrapezoid, nVII: facial motor, BötC: Bötzinger complex, preBötC: preBötzinger Complex (orange dotted circle), rVRG: rostral ventral respiratory group, and LRt: lateral reticular nuclei.(B-G) Lineage (B–E) and neuronal projection (F, G) mapping of WT (*Atoh1*$^{Cre/+}$; *Tau*$^{mGFP\text{-}nLacZ}$) and *Atoh*-null (*Atoh1*$^{Cre/-}$; *Tau*$^{mGFP\text{-}nLacZ}$) brainstems at E18.5.The somas (nLacZ) of *Atoh1* descendants in the *Atoh1*-null (C) brainstems are either mislocalized(RTN, white arrowhead)or lost(Sp5I and LRt nuclei). The expression of RTN

neuronal lineage markersPhox2b and Lbx1 in WT (D) and *Atoh1*-null (E) are similar. The Atoh1-dependent projections (mGFP shown in green) originate from rostral (white open arrowheads) and caudal (white arrowheads) Atoh1 populations that innervate the preBötC (orange dotted circle, marked by somatostatin, Sst in red)are detected in WT(F) but lost in *Atoh1*-null (G).Neurites of the RTN neurons in *Atoh1*-null mice do not connect with the pre BötC and accumulate at the dorsal surface of nVII (G, yellow arrowhead). All images are shown in sagittal sections. Scale bars represent 100 μm.

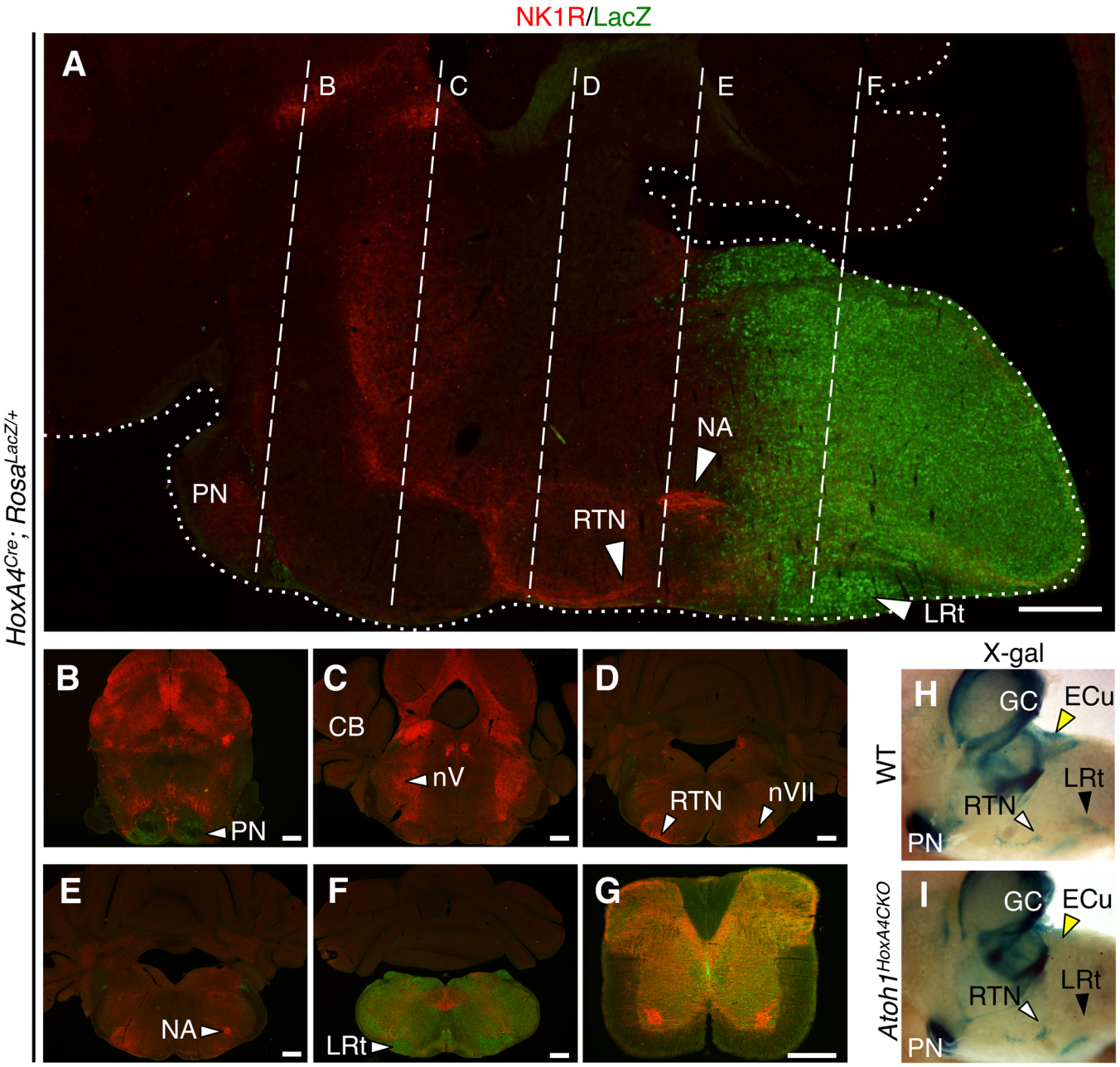

Figure 2. Characterization of the *HoxA4*^{Cre} allele and selective removal of *Atoh1* from the caudal rhombomeres

(A-G)Cre recombinase expression of the *HoxA4*^{Cre} driver line was evaluated by crossing *HoxA4*^{Cre} with *Rosa*$^{LacZ/LacZ}$ reporter mice followed by sagittal (A) and coronal (B-G) sections of 3-week-old mice. Sections were co-stained with LacZ(green, indicates Cre activity) and *neurokinin 1 receptor*(NK1R marked in red as molecular landmark). (A) Sagittal sections showing that *HoxA4*^{Cre} activities are restricted to structures posterior to rhombomere 7 and spared the NK1R positive RTN neurons. (B-F) Coronal sections correspond to the levels indicated by white dotted line in (A). A small *HoxA4*^{Cre}–expressing subpopulation migrates anteriorly to the pontine nucleus (white arrowhead in B).(G) The *HoxA4*^{Cre} allele also targets neurons within the spinal cord. (H, I)Side view of the whole mount X-gal staining (rostral to the left) to trace the *Atoh1* lineages in WT(H, *Atoh1*$^{LacZ/+}$)

and *Atoh1*^{HoxA4CKO}(I) brainstems at E18.5. LacZ activity marks the *Atoh1* descendants. The Atoh1–dependent ECu (yellow arrowheads) and LRt nuclei (black arrowheads) fail to form due to the loss of *Atoh1* in the *HoxA4* lineages, while the RTN neurons are unaffected and migrate normally to the ventral medullar surface (white arrowheads). The anterior RL–derived Atoh1 neurons, such as cerebellar granule cells and pontine nucleus, are also preserved due to different rhombomeric origins, confirming the specificity of the transgenic Cre alleles. Abbreviations: CB: cerebellum, ECu: external cuneate, GC: cerebellar granule cells, LRt: lateral reticular, NA: nucleus ambiguous, nV: trigeminal motor, nVII: facial motor, PN: pontine, and RTN: retrotrapezoid nuclei. Scale bars represent 500 μm.

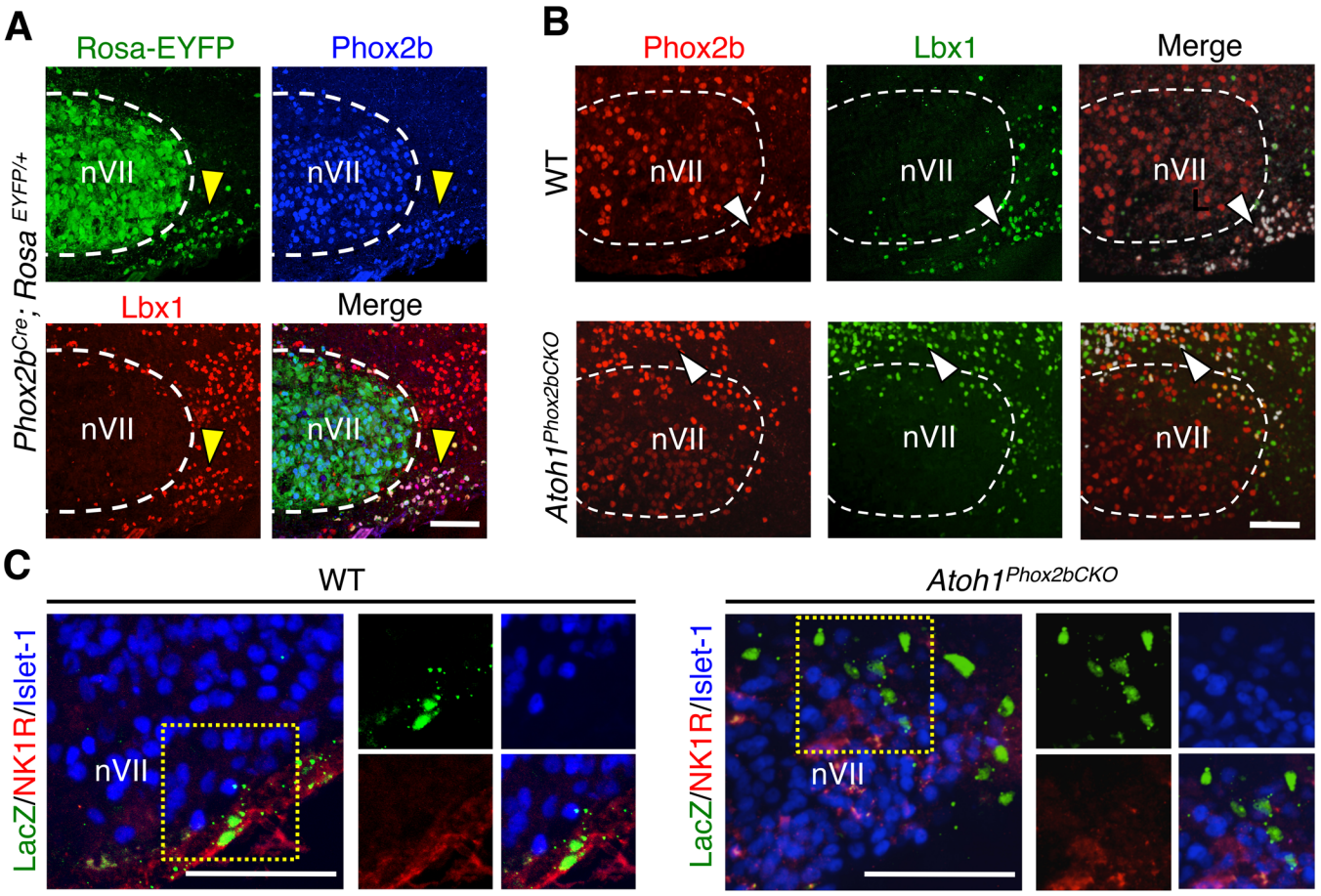

Figure 3. Atoh1is cell–autonomously required for RTN ventral migration and differentiation

(A) Expression pattern of the *Phox2b*^{Cre} line as assessed by *Rosa*$^{EYFP/EYFP}$ reporter showing that the Cre (*EYFP*, green), Phox2b (blue), and Lbx1 (red) in the RTN neurons (yellow arrowheads)are highly overlapped.(B)The RTN neurons of WT and *Atoh1*^{Phox2bCKO} brainstems express lineage markers Phox2b (red) and Lbx1 (green) in anAtoh1–independent manner (white arrowheads), despite the migration defect in the *Atoh1*^{Phox2bCKO} brainstem. Images in A and B are sagittal sections from E18.5 brainstems. (C) Expression of RTN differentiation marker NK1R (red)is lost in *Atoh1*^{Phox2bCKO} RTN neurons (LacZ, green)as shown in coronal sections from E16.5 brainstems. RTN neurons in the overlaid images (left) are outlined with yellow dotted box, and markers are shown individually (right). All scale bars represent 100 μm.

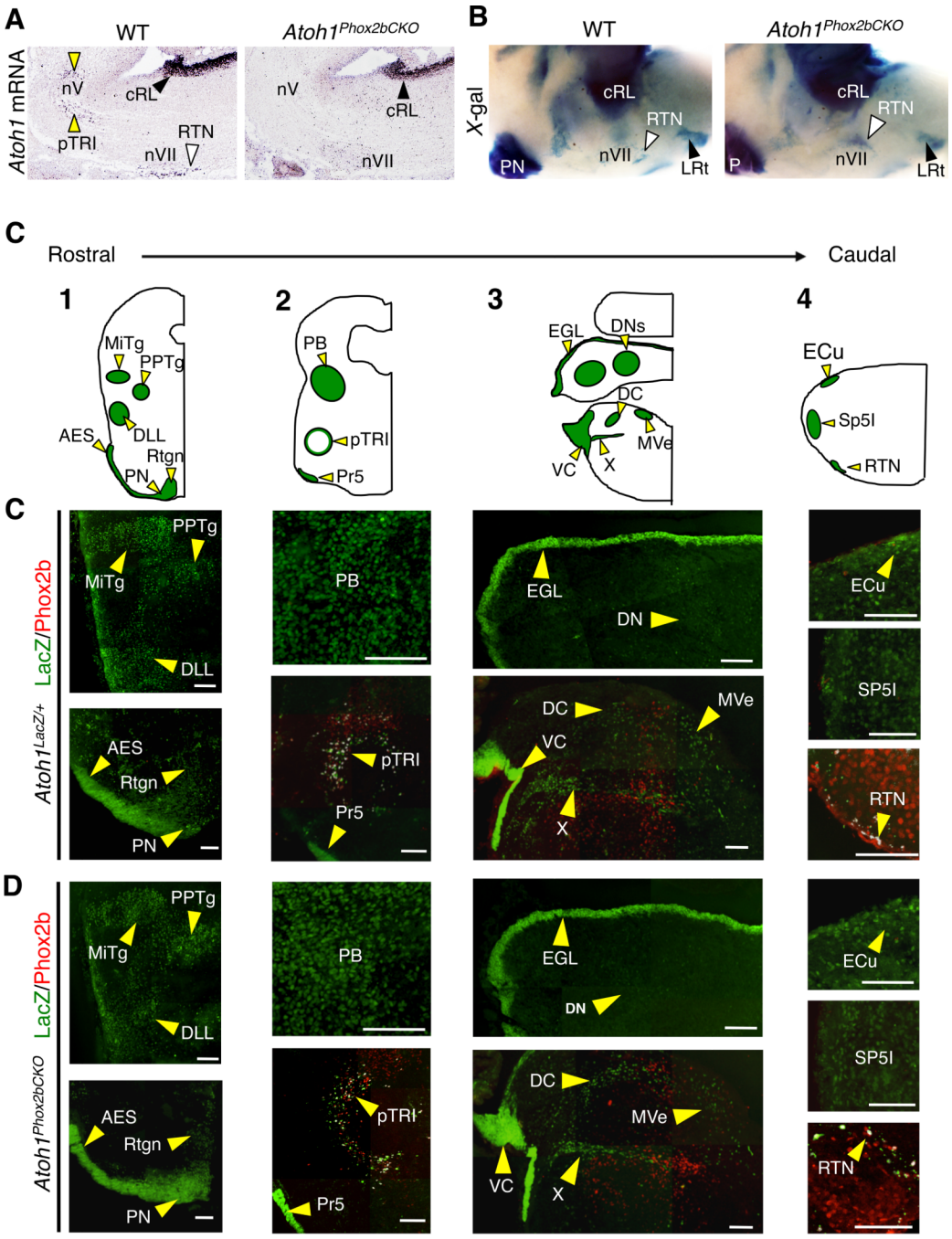

Figure 4. *Phox2b*^{Cre} allele selectively targets paramotor neurons and spares the rhombic lip (RL)–derived Atoh1populations

(A)*in situ* hybridization of E14.5 WT and *Atoh1*^{Phox2bCKO} sagittal brainstem sections (rostral to the left) confirming *Phox2b*^{Cre} selectively removes *Atoh1* mRNA from the RTN (white arrowhead) and the pTRI (yellow arrowheads) neurons. The caudal rhombic lip (cRL, black arrowheads) progenitors retained *Atoh1* expression in the *Atoh1*^{Phox2bCKO} brainstem. (B)Side view of the whole mount X-gal staining (rostral to the left) to trace the *Atoh1* lineages in WT (*Atoh1*$^{LacZ/+}$) and *Atoh1*^{Phox2bCKO} brainstems at E18.5. LacZ activity marks the *Atoh1* descendants. The RTN neurons are mislocalized in *Atoh1*^{Phox2bCKO} mice, while the RL lineages remain anatomically intact. (C) Schematics of the Atoh1 hindbrain lineages

(shown in green, indicated by yellow arrowheads). All coronal hemisections (1–4, rostral to caudal) are oriented with lateral to the left. (D, E) Serial coronal sections from E16.5 *Atoh1*$^{LacZ/+}$ (D) and *Atoh1*^{Phox2bCKO} (E) brainstems at approximate levels 1–4 in (C). Sections were co-stained with LacZ (green, *Atoh1* lineages indicated by yellow arrowheads) and Phox2b (red). The RL-derived Atoh1 populations remain anatomically intact in the *Atoh1*^{Phox2bCKO} brainstems, and the RTN neurons are dorsally misplaced in the *Atoh1*^{Phox2bCKO} brainstem (co-localization of LacZ and Phox2b double positive cells are shown in white). Abbreviations: AES: anterior precerebellar extramural stream, DC: dorsal cochlear, DLL: dorsal lateral lemniscal, DNs: deep cerebellar, ECu: external cuneate, EGL: external granule layer, MiTg: microcellular tegmental, MVe: medial vestibular, PB: parabrachial, PN: pontine, PPTg: pedunculopontine, Pr5: principal sensory trigeminal, pTRI: paratrigeminal, Rtgn: reticulotegmental, RTN: retrotrapezoid, Sp5I: interpolar division of the spinal trigeminal nucleus, VC: ventral cochlear, and X: vestibular nuclei. Scale bars represent 100 μm.

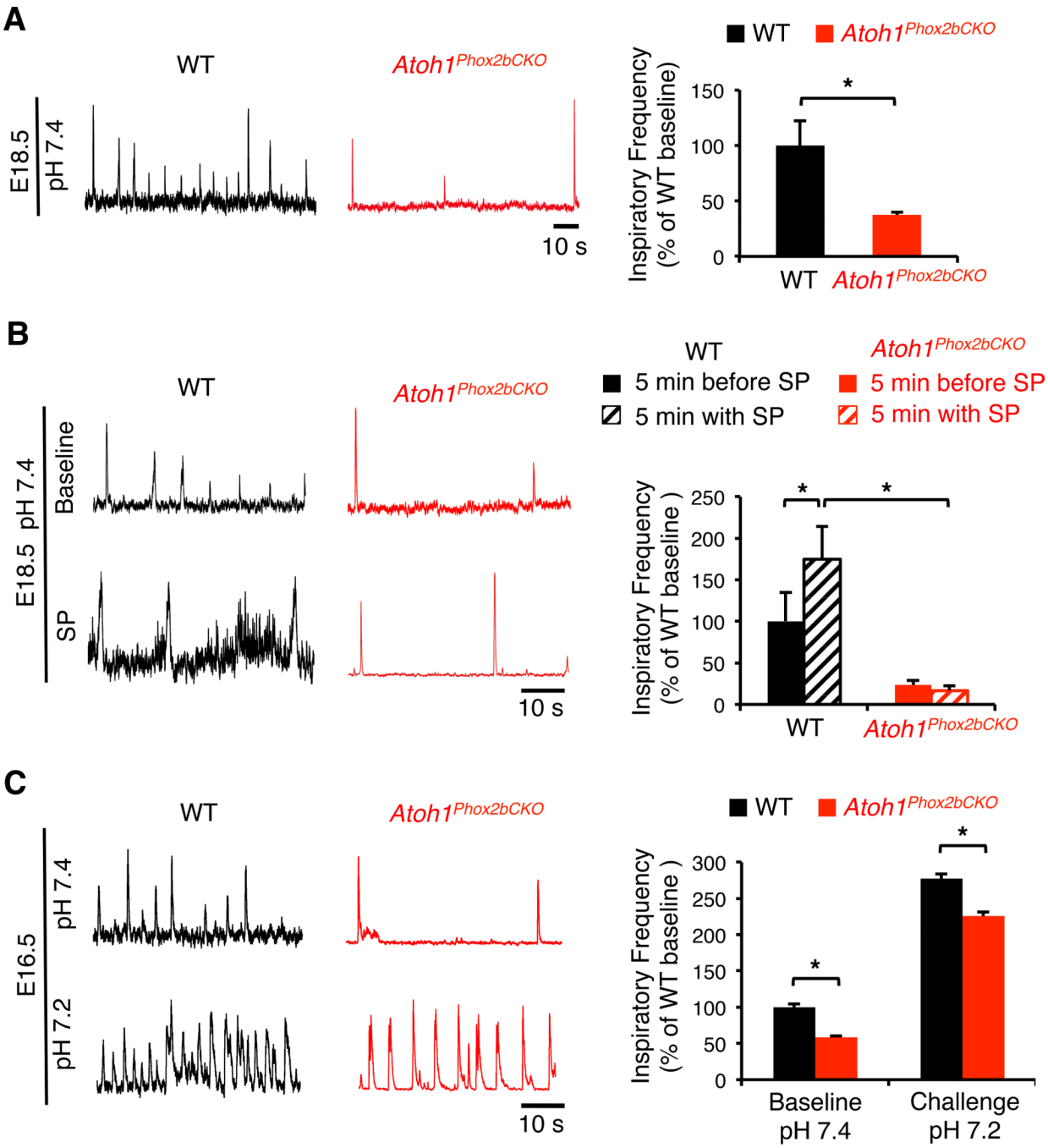

Figure 5. Atoh1–mediated RTN development is involved inneonatal inspiratory rhythm generation

(A)Neonatal *Atoh1*^{Phox2bCKO} mice generate significantly slower inspiratory motor activity when compared to WT. The integrated suction electrode traces of E18.5 WT (n=9) and *Atoh1*^{Phox2bCKO} (n=5) *en bloc* preparations represent the fictive respiratory motor rootlet activity, quantified in a bar graph(*p<0.05, mean values ± SEM, independent samples t–test).(B) Substance P (SP) does not trigger inspiratory–related motor activity in *Atoh1*^{Phox2bCKO} brainstems, which is normally seen in WT preparations. Electrode traces were generated during baseline and brainstem application of 1μM SP in E18.5 WT and

Atoh1^{Phox2bCKO} *en bloc* preparations. The bursting frequency 5 minutes before and after SP treatment was quantified in the bar graph.

(C)Embryonic *Atoh1*^{Phox2bCKO} mice show significantly slower inspiratory motor activity compared to WT under both baseline (pH 7.4)and acidosis (pH 7.2) environments. The integrated suction electrode traces of E16.5 WT (n=7) and *Atoh1*^{Phox2bCKO} (n=11) *en bloc* preparations (left) represent the fictive respiratory motor rootlet activity, quantified in a bar graph (right, *$p<0.001$, mean values ± SEM, independent samples t–test).

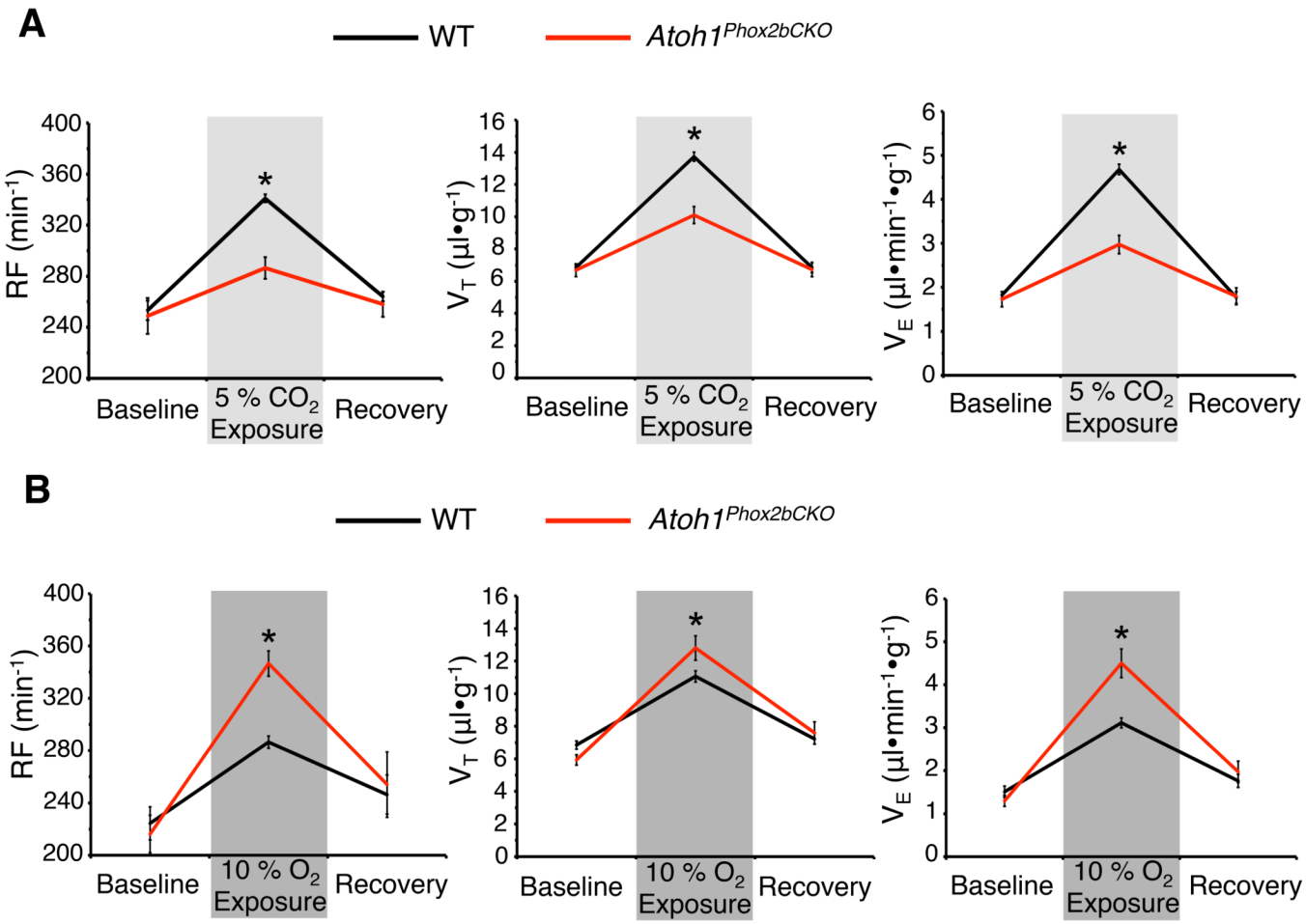

Figure 6. *Atoh1*^{Phox2bCKO} survivor mice develop abnormal chemosensory responses in adulthood

Graphs show respiratory frequency (RF), tidal volume (V_T) and minute ventilation (V_E) of 3 month old *Atoh1*^{Phox2bCKO} mice (n=9) as well as WT (n=21) when challenged with hypercapnia (5% CO_2, A) or hypoxia (10% O_2, B). *Atoh1*^{Phox2bCKO} mice have a significantly weaker response to hypercapnia (A) but have a stronger response to hypoxia (B). Shown are the mean values ± SEM over 20 minutes of normoxic baseline, 5 minutes of gas challenge and 15 minutes of normoxic recovery phases.*p<0.05, ANOVA.